J. COMBIN. MATH. COMBIN. COMPUT. 127a (2025) 5823--5850

Journal of Combinatorial Mathematics and Combinatorial Computing
www.combinatorialpress.com/jcmcc

Combinatorial Press

Theoretical study on the design of improved dynamic characteristics of wind-resistant performance of large-span steel structures based on topology optimization

Qiang Li[1,✉], Peiwen Yu[1], Danni Chen[1]

[1] *School of Human Settlements and Civil Engineering, Xi'an Eurasia University, Xi'an, Shaanxi, 710065, China*

ABSTRACT

Large-span steel structures are prone to wind vibration under wind loads, which affects the safety and performance of the structure, and wind vibration control is the key to its design. This paper takes the large-span steel structure as the research object, firstly introduces the theory and method related to wind vibration control analysis, constructs the topology-optimized inertial capacitance damper-controlled wind vibration response dynamic equation of super high-rise building to analyze the influence law of wind speed and wind direction on the dynamic characteristics of the structure, and then further strengthens the vibration control ability of the structure through reasonable arrangement and parameter adjustment. The deformation of ETABS model in y-direction is larger than that in x-direction under 50-year wind load, and the maximum displacements in y- and x-directions are 18.72 mm and 11.65 mm, respectively. The y-direction interstory displacement angle meets the code requirement limit (2.65×10-4). The amplitude of the acceleration time-range curve of its top floor structure is between ±0.08, which meets the requirements for comfort. The optimization of the reinforcement layer using continuum topology optimization is better than the optimization of the optimal location arrangement according to finite element software. The results of node displacements and inter-story displacement angles of each story of the modified structural model under wind load meet the limits of top story displacement and inter-story displacement angle, and the performances are similar to those of the extended-arm truss structural model.

Keywords: inertial capacitive damper, dynamic equation of wind vibration response, topology optimization, wind vibration control, long-span steel structure

1. Introduction

The so-called large-span steel structure refers to the structure that has a three-dimensional shape that is not suitable for decomposition into a planar structural system, has three-dimensional stress

✉ Corresponding author.
E-mail address: Liqq480429@163.com (Q. Li).
Received 25 March 2024; Revised 05 June 2024; Accepted 15 December 2024; Published Online 15 April 2025.
DOI: 10.61091/jcmcc127a-323

performance and can span a large space, and works in space under the action of loads [1]. Among them, space structure can be divided into three basic types: solid structure, lattice structure, and tension structure. Solid structure class has thin shell structure and folded plate structure, they are generally reinforced concrete solid structure; grid structure class consists of net frame structure and net shell structure, generally by the rod according to a certain law of the composition of the grid of high-order superstatic space rod system structure; tension structure class consists of suspension structure and film structure, generally through the pre-tension applied to the cable or membrane after the formation of the structural system [2-5]. In addition to the above three basic types, the structure that concentrates the advantages of the above two or several structures is called hybrid structure or hybrid structure, and this kind of structure has become one of the hot spots of research in recent years.

With the development of steel structure, the span of large-span steel structure gradually increases, the structure becomes more and more complex, the application of high-strength steel is widely used, and the design requirements are improved [6]. In addition, its dynamic structure is also gradually revealed, for example, a large-span structure is a stadium, gymnasium, but also to take into account the role of exhibition halls and multi-function halls, the use of more convenient [7]. The rapid development of large-span steel structure is mainly due to its beautiful spatial form, reasonable force and low steel consumption, and its reasonable shape itself can resist part of the external loads and achieve mechanical balance [8-10]. Because of this, the large-span steel structure has more and more influence on the modern building structure, and has become one of the important symbols to measure the scientific and technological level of a country. The stability and reliability of large-span steel structures is a very important design consideration to avoid serious accidents such as collapse of the structure during stressing [11]. Wind is one of the main factors leading to the stresses on building structures, which is mainly manifested in three aspects: wind pressure, wind vibration, and wind load, especially in large-span structures such as high-rise buildings and bridges [12-13].

The aim of this paper is to carry out a theoretical study on the improved design of the dynamic characteristics of the wind performance of a large-span steel structure through the coordinated action of topology optimization and inertial capacitance damper TMDI. In the study, the mechanism of the influence of wind speed and direction changes on the dynamic response of the structure is deeply analyzed. Then the topology optimization technique is used to optimize the shape and layout of the structure to reduce the wind response of the structure. In addition, combined with the characteristics of the inertial capacitance damper TMDI, a strategy to optimize its arrangement and parameters is proposed to further improve the wind vibration control effect of the structure. Through theoretical analysis and numerical simulation, the effectiveness of the proposed theoretical method is verified, and new ideas and methods are provided for the wind-resistant design of large-span steel structures.

2. Overview

Large-span steel structures are also affected by external factors, resulting in internal and surface force deformation, such as literature [14] analyzed the thermal performance of large-span steel structures under solar radiation through numerical simulation methods, showing that the effect of solar radiation on the structure is less than the seasonal temperature difference, and its internal force is released through the deformation of the grid structure. For large-span steel structures more common and numerical must be bridges, and wind, as a natural phenomenon, is unavoidable, so many scholars have studied large-span structures under wind. Literature [15] analyzed the stability of lightweight steel structures of super high-rise buildings under the influence of wind, including the internal stress analysis of lightweight steel structures in strong winds using stress model-based calculations, the analysis of building node data by over-filtering calculations, and the stiffness equations for the resistance reliability analysis of lightweight steel structures under internal pressure and wind pressure. Literature [16] constructed a fatigue reliability evaluation framework for large-span steel bridges under random traffic and wind loads using stress analysis, which showed that traffic and wind loads have an effect on their fatigue reliability, especially on the upper and lower chords at the quarter-span of the main truss of the bridge. Literature [17] analyzed wind vibration data from long-term monitoring of large-span bridges by cluster analysis, and the unsteady wind speed significantly affected the vortex-excited vibration modes along the span direction. Literature [18] used Monte Carlo technique to analyze the flutter reliability of large-span suspension bridges under tropical cyclone wind conditions and predicted the probability of flutter failure by wind duration, bridge surface roughness and length, and flutter analysis model combination. Literature [19] analyzed the acceleration response calculated by multimodal chattering theory, vibration characteristics and wind characteristics from long-term monitoring data, and wind spectra derived under design rules using chattering response analysis, and comparisons revealed that this analysis was lower than the measured response for chattering measurements. These studies, the reliability, stability, and bridge shaking vibration under wind were evaluated and analyzed by stress analysis, cluster analysis, and shaking vibration response analysis for large block are bridges. This is far from enough for the design of wind-resistant structures with large-span steel structures and lacks the study under wind dynamic conditions.

3. Improved design method for dynamic characterization of wind resistance of long-span steel structures

3.1. Theories and methods related to wind vibration control analysis

3.1.1. Structural wind design theory. In engineering calculation and design, the wind pressure is used to express the magnitude of the action of wind load [20], combined with the relevant knowledge of fluid mechanics, the low-speed movement of air is regarded as an incompressible fluid, and when the fluid mass point is in the same horizontal line for stable movement, its energy expression is:

$$w_a V + \frac{1}{2} m v^2 = C \tag{1}$$

Where, $w_a V$ for the static pressure energy $(kN \cdot m)$, $\frac{1}{2} m v^2$ for the kinetic energy $(kN \cdot m)$, C is a constant, w_a for the static pressure per unit area $\left(kN / m^2\right)$, V for the volume of the air mass $\left(m^3\right)$, m for the mass of the moving fluid mass (t), v for the wind speed (m/s).

The Bernoulli equation can be derived by dividing both sides of the above equation by V from $m = \rho V, \rho$, which is the density of the air mass $\left(t / m^3\right)$:

$$w_a + \frac{1}{2} \rho v^2 = C_1 \tag{2}$$

Then the wind pressure per unit area of free airflow:

$$w = C_1 - w_a = \frac{1}{2} \rho v^2 \tag{3}$$

When the structure is subjected to pulsating wind load for dynamic calculation, after obtaining the time course sample data, can be processed through the peak factor method to meet the calculation of the required guarantee rate of the peak of the dynamic response, the following formula (4) to obtain the peak data for the structure of the dynamic response of the performance indexes of the calculation or analysis and comparison.

$$Y_{\max} = Y + g R_Y \tag{4}$$

Where, $Y_{\max}$ represents the peak value of the effect during wind vibration of the structure, which can be various time-range response parameters such as displacement, velocity, acceleration, etc., Y

and R_Y represent the mean and standard deviation of the time-range sample data, respectively, and g represents the peak factor.

3.1.2. Analytical model for structural wind vibration control. Under the wind load $P(t)$, the extension arm damping control model [21] is shown in Fig. 1 and the TMD control model is shown in Fig. 2. It consists of a frame-core model with dampers arranged in the reinforcement layer of the reach arm. The number of extensible arm dampers are arranged. Usually, the TMD system is set up in the floor near the top of the structure, and the mass of the TMD is m_T, the damping is c_T, and the stiffness is k_T. The structure produces a displacement $u(t)$ and the TMD produces a displacement $w(t)$ under wind loading.

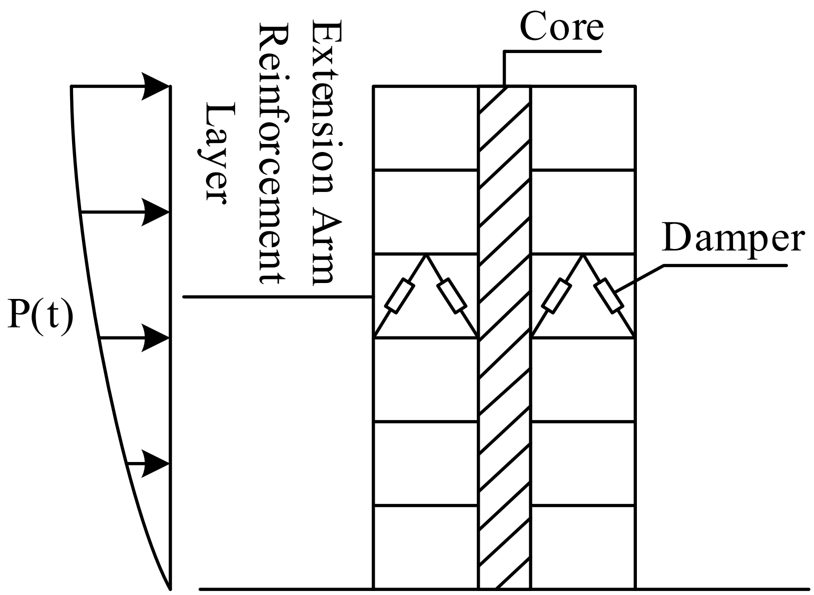

Fig. 1. The arm damping control model

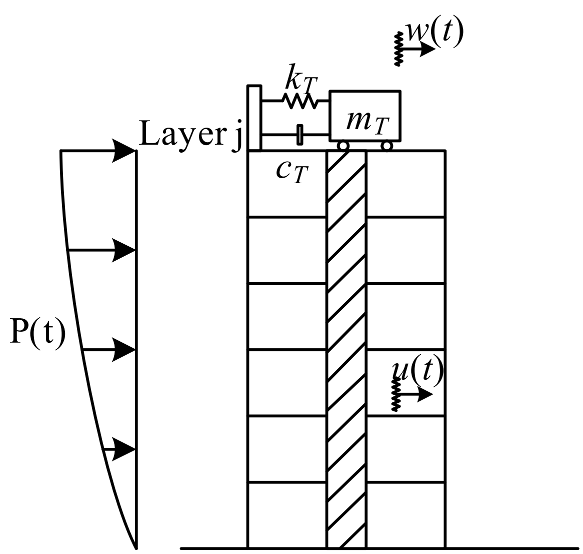

Fig. 2. TMD control model

For a super high-rise structure with dampers, the governing equations of the structure during wind loading can be expressed as the following equation:

$$\begin{cases} M\ddot{u}(t) + C\ddot{u}(t) + Ku(t) = P(t) + H\left(C_T\dot{w}(t) + K_T w(t)\right) \\ M_T\ddot{w}(t) + C_T\dot{w}(t) + K_T w(t) = -M_T H^T \ddot{u}(t) \end{cases} \tag{5}$$

$w(t)$ is the displacement vector generated by the damper, $w(t)$ and $u(t)$ corresponding to the first-order derivative is the velocity vector, the second-order derivative is the acceleration vector; M, C, K, M_T, C_T, K_T are the mass, damping, and stiffness matrices of the main structure and the damper, respectively; H is the position matrix of the damper, which is used to represent the floor where the damper is located; $H^T = [0,\cdots,0,1,0,\cdots,0]_{1\times N}$, where 1 is the position vector, and 1 in the k th column represents that the damper is set at the kth floor of the structure.

For the super high-rise structure with TMD, by substituting the specific parameters m_T, c_T, k_T of TMD into the above equation and setting the TMD system set at the j th floor and the position vector as H_j, equation (5) can be rewritten as:

$$\begin{cases} M\ddot{u}(t) + C\dot{u}(t) + Ku(t) = P(t) - H_j\left(m_T\ddot{w}(t) + m_T H^T \ddot{u}(t)\right) \\ m_T\ddot{w}(t) + c_T\dot{w}(t) + k_T w(t) = -m_T H_j^T \ddot{u}(t) \end{cases} \tag{6}$$

That is the control equation of the TMD system. According to the principle of energy balance, multiplying both ends of Eq. (5) by the relative displacement vector $du^T(t)$ and integrating, it can be obtained:

$$\begin{aligned} &\int \dot{u}^T(t)M\ddot{u}(t)dt + \int \dot{u}^T(t)C\dot{u}(t)dt + \int \dot{u}^T(t)Ku(t)dt \\ &= \int \dot{u}^T(t)P(t)dt + \int \dot{u}^T(t)HC_r\dot{v}(t)dt + \int \dot{u}^T(t)HK_r w(t)dt \end{aligned} \tag{7}$$

Relative energy equations are obtained to represent the structural energy at any moment in time:

$$E_{in} = E_k + E_c + E_e + E_{tran} \tag{8}$$

$$E_{tran} = E_c' + E_e' \tag{9}$$

Among them:

$$E_{in} = \int \dot{u}^T(t)P(t)dt \tag{10}$$

$$E_k = \int \dot{u}^T(t)M\ddot{u}(t)dt \tag{11}$$

$$E_e = \int \dot{u}^T(t)C\dot{u}(t)dt \tag{12}$$

$$E_e = \int \dot{u}^T(t)Ku(t)dt \tag{13}$$

$$E_c' = -\int \dot{u}^T(t)HC_T\dot{w}(t)dt \tag{14}$$

$$E_e' = -\int \dot{u}^T(t)HK_r w(t)dt \tag{15}$$

That is, at any moment, the total energy input into the structure by wind load E_{in} is converted into structural kinetic energy E_k, potential energy E_e, the structure's own damping energy dissipation E_c, and the energy converted by the damper E_{tran}, of which E_{tran} consists of the damping part of the damping system energy dissipation E_c' and potential energy E_e'. E_k, E_e and E_e^* can only convert the energy of the main structure, but cannot dissipate the energy, so the energy dissipation of the structure mainly relies on the damping of the main structure itself and the damping in the damper system.

However, in the structural wind vibration calculation, it is usually assumed that the structure is always in the elastic phase, when E_c only accounts for a small part of the total energy of the wind vibration, and the structure mainly relies on the dampers for energy dissipation, i.e.:

$$E_{in} = E_c{}' = -\int \dot{u}^T(t) H C_T \dot{w}(t) dt \tag{16}$$

In this paper, the finite element software ETABS is used for modeling and calculation to carry out the subsequent analysis and optimization of the wind vibration control scheme.

When ETABS is used to establish a three-dimensional finite element model for analysis, i.e., a computational model consisting of a spring k and damping c in series, the nonlinear force-deformation relationship is:

$$f_d = kd_k = c\dot{d}_c \tag{17}$$

$$d = d_k + d_c \tag{18}$$

where d is the total deformation between points i and j, k is the spring stiffness, d_k is the spring deformation, c is the damping coefficient, and d_c is the damper deformation. When k is large enough and d_k is small enough, then $d = d_c$, then $f_d = c\dot{d}_c$, where c is the damping of the damper C. Using this principle, the effect of a viscous damper can be simulated by setting the spring stiffness to a larger value (usually $10^2 \sim 10^4$ times) in the software.

TMD optimal parameter design method for undamped single-degree-of-freedom structures:

$$\lambda = \frac{1}{1+\mu}, \xi_{opt} = \sqrt{\frac{3\mu}{8(1+\mu)}} \tag{19}$$

where $\lambda = \omega_1 / \omega_1$ is the frequency ratio, ω_1 is the TMD frequency, ω_1 is the first stage frequency of the main structure, μ is the mass ratio; ξ_{opt} is the optimal damping ratio of the TMD.

The undamped structure under the action of white noise excitation, the parameter value formula of TMD can be rewritten as:

$$\lambda = \sqrt{\frac{(1-\mu/2)}{1+\mu}}, \xi_{opt} = \sqrt{\frac{\mu(1-\mu/4)}{4(1+\mu)(1-\mu/2)}} \tag{20}$$

Optimal TMD parameter formulation for damped structures:

$$\lambda = \frac{1}{1+\mu}\left(1-\zeta_p\sqrt{\frac{\mu}{1+\mu}}\right), \xi_{opt} = \frac{\zeta_p}{1+\mu} + \sqrt{\frac{\mu}{1+\mu}} \tag{21}$$

Optimal parameter theory is chosen to optimize the values.

3.1.3. Theory of structural topology optimization. For the extended-arm truss structure in the reinforced floor of a super high-rise building, one of the bays of the frame with extended-arm members is taken, and the local arrangement of the truss can be optimized by the principle of continuum topology optimization [22-23]. The example of continuum algorithm is shown in Fig. 3, let a continuum side length is B, the upper end is free, acting two centralized forces P, and the bottom two points are fixed support, the continuum is topology optimized, and after stress analysis, the part with the smallest value of stress will be controlled by the rejection rate and deleted, and the cycle is continuous to reach the objective function. The topology optimization solution process is shown in Fig. 4. An optimized topological shape can be obtained, which reaches the fullness of the stress in each block of the member under a certain external force, and is able to exert the mechanical properties of the material as much as possible.

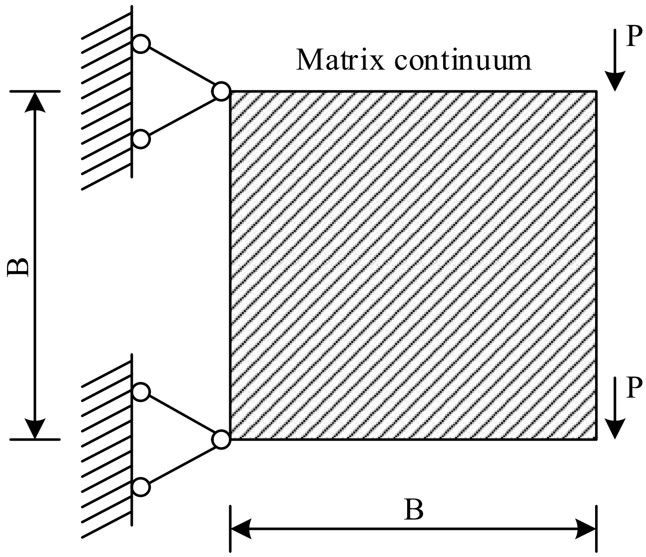

Fig. 3. Continuous example

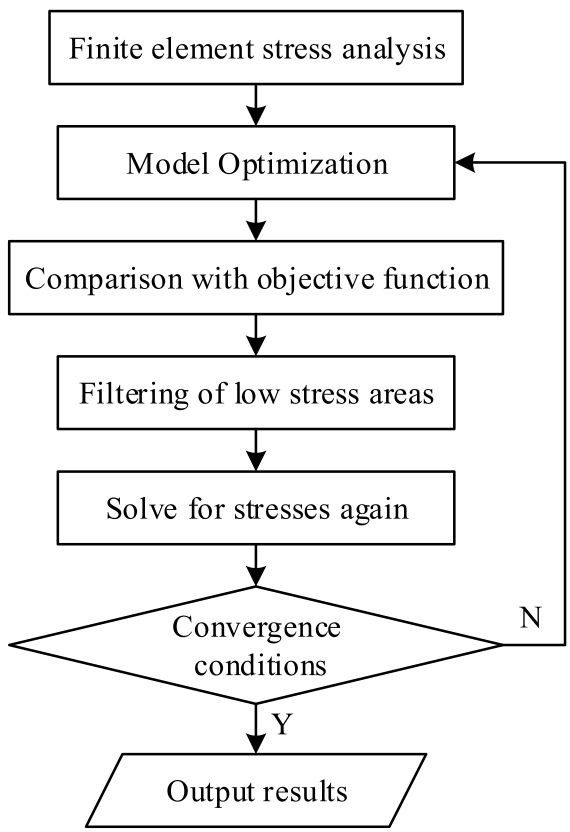

Fig. 4. Topology optimization process

The topology optimization solution is shown in Fig. 5, where the material distribution inside this continuum is optimized to four rods, which is the most stress-full arrangement in the local structure. The arrangement form of the extended arm truss and its damper can be optimized.

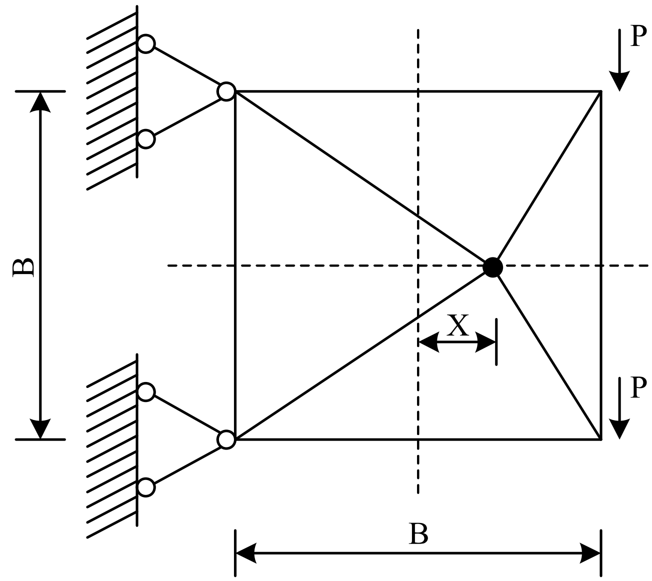

Fig. 5. Topology optimization solution

3.2. Topology optimized dynamic equations for wind vibration response of high-rise buildings

The suspension mounting of the inertial capacity damper TMDI is shown in Fig. 6. A suspension damping device is suspended from the t st floor slab of the super high-rise building structure with a damping coefficient denoted by c and a stiffness of the suspension structure denoted by k, and an accessory mass of mass m is attached below it. The attached mass is connected to the $t-p$ th floor slab of the structure by means of a number of inertia packages connected in parallel. The system is subjected to wind loads with a concentrated force of $F_i(i=1,2,3,\ldots,n)$ distributed at the points of the concentrated mass.

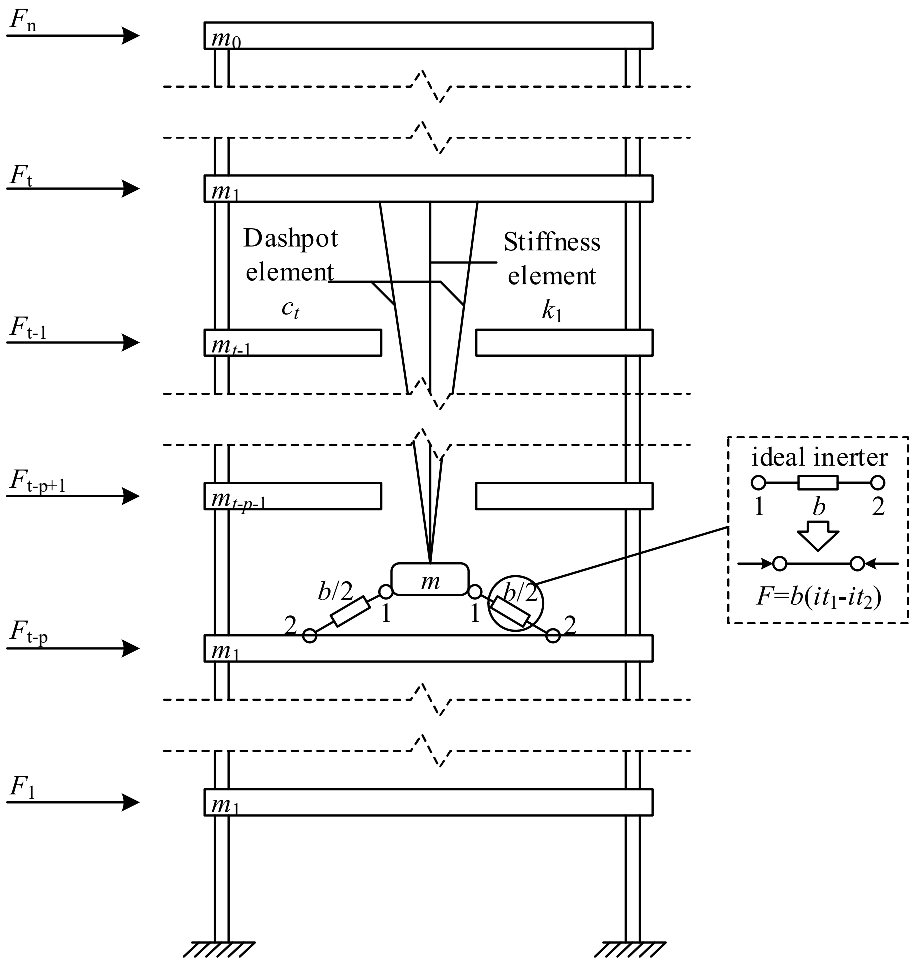

Fig. 6. Tmdi-superhigh-rise building coupling linear centralized mass model

Based on D'Alembert's principle, the linear structural equations of motion for this system can be expressed as:

$$M\ddot{u}(t)+C\dot{u}(t)+Ku(t)=p(t) \tag{22}$$

In the above equation, $\ddot{u}(t)$, $\dot{u}(t)$ and $u(t)$ denote the acceleration vector, velocity vector and displacement vector of each degree of freedom of the structure at the moment of t, and $p(t)$ denotes the aerodynamic force vector acting on each degree of freedom of the structure at the moment of t. When the upper part of the inertial volume damper TMDI is suspended from the t th floor slab and the lower part is connected to the $t-p$ th floor slab by the inertial volume device, the number of topological layers of this TMDI is defined as "$-p$". Now M, C, K in the above equation can be specified as:

$$\begin{aligned}
M &= M_s^{n+1}+\left(m_t+b\right)\times I_{n+1}1_{n+1}^T+b\times I_{1-p}1_{t-p}^T-b\times\left(1_{n+1}1_{t-p}^T+1_{n+1}^T I_{t-p}\right)\\
C &= C_s^{n+1}+c_1\times\left(1_{n+1}1_{n+1}^T+1_1 1_1^T-I_1^T 1_{n+1}-I_1 1_{n+1}^T\right)\\
K &= K_s^{n+1}+k_c\times\left(1_{n+1}1_{n+1}^T+1_1 1_1^T-I_1^T 1_{n+1}-1_1 1_{n+1}^T\right)
\end{aligned} \tag{23}$$

In Eqs. M_s^{n+1}, C_s^{n+1}, and $K_s^{n+1}\in R^{(n+1)(n+1)}$ above, a square matrix of order $n+1$ is formed by adding a row and column of zeros to the last row and column of the matrix, respectively, based on the mass, damping, and stiffness matrices $\left(M_s,C_s,K,\in R^{*N}\right)$ of the initial structure without TMDI. The elements of the localization vector $1_i\in R^{(n+1)4}$ in Eq. 6 are all zeros, except for the i th element, which is 1. The transpose symbol is the superscript T in Eq.

The damping matrix of the structure becomes a non-orthogonal damping matrix because of the TMDI installed in the building, so the system of second-order linear differential equations has to be solved in the state space by using the method of complex modal superposition with the following equation:

$$A\dot{z}(t)+Bz(t)=f(t) \tag{24}$$

Among them:

$$A=\begin{bmatrix} C & M \\ M & 0 \end{bmatrix}, B=\begin{bmatrix} K & 0 \\ 0 & -M \end{bmatrix}, f(t)=\begin{bmatrix} p(t) \\ 0 \end{bmatrix}, z(t)=\begin{bmatrix} u(t) \\ \dot{u}(t) \end{bmatrix} \tag{25}$$

From the above equations, it can be known that when the excitation is applied at the q st degree of freedom of the super tall building structure, the displacement response frequency response function and the acceleration response frequency response function of the p nd degree of freedom of the structure are expressed:

$$\begin{aligned} H_D^M(j\omega)&=\sum_{k=1}^{N}\left(\frac{\varphi_{pk}\varphi_{qk}}{a_k\left(j\omega-s_k\right)}+\frac{\varphi_{pk}^{*}\varphi_{qk}^{*}}{a_k^{*}\left(j\omega-s_k^{*}\right)}\right) \\ H_A^M(j\omega)&=\sum_{k=1}^{N}\left(\frac{-\omega^2\varphi_{pk}\varphi_{qk}}{a_k\left(j\omega-s_k\right)}+\frac{-\omega^2\varphi_{pk}^{*}\varphi_{qk}^{*}}{a_k^{*}\left(j\omega-s_k^{*}\right)}\right) \end{aligned} \tag{26}$$

where the value corresponding to the p nd degree of freedom in the k st order complex vibration mode of the super tall building structure is denoted by φ_{pk}, the value corresponding to the q th degree of freedom is denoted by φ_{qk}, φ_{pk}^{*} and φ_{qk}^{*} are the corresponding conjugate values, s_k and s_k^{*} are the k th order eigenroot and the corresponding conjugate value of the structure, and a_k and a_k^{*} can be calculated by the following equation:

$$\Phi^T A\Phi = diag\left\{a_1 \quad L \quad a_k \quad a_l^{*} \quad L \quad a_k^{*}\right\} \tag{27}$$

where the eigenmatrix consisting of eigenvectors ϕ_i is denoted by Φ.

On the basis of the complex modal superposition method, the structural response timescale $z(t)$ expression in the state space is as follows:

$$\begin{aligned} z(t)&=\sum_{i=1}^{2n+2}\phi_i q_i(t) \\ z(t)&=\sum_{i=1}^{n+1}\left(\frac{\phi_i}{a_i}\int_0^t F_i(\tau)e^{f_i(t-r)}d\tau+\frac{\phi_i^{*}}{a_i^{*}}\int_0^t F_i^{*}(\tau)e^{f_i^{*}(t-r)}d\tau\right) \end{aligned} \tag{28}$$

where the i st order complex mode shapes of the structure are denoted by ϕ_i and the corresponding conjugate values are denoted by ϕ_i. The expression for the i th order generalized force and the corresponding expression for the conjugate value are shown below:

$$\begin{aligned} F_i(t)&=\phi_i^T f(t) \\ F_i^{*}(t)&=\phi_i^{*T} f(t) \end{aligned} \tag{29}$$

After the wind-induced displacement response and acceleration response timescales of the super high-rise building structure are obtained by calculation, the equivalent static wind load of the structure can be calculated by using the displacement magnitude factor method with the following expression:

$$F_{csw1}(z)=G(z)\overline{P}(z) \tag{30}$$

In the above equation, the average aerodynamic force is denoted by $\bar{P}(z)$, and this value can be obtained from wind tunnel tests and field measurements. The displacement amplitude factor at different heights is denoted by $G(z)$, and the value can be obtained by the expected extreme and mean values of the displacement response of the super high-rise construction structure, which is expressed as:

$$G(z)=\frac{\hat{D}(z)}{\bar{D}(z)} \tag{31}$$

In the formula, the average value of the displacement response of the super high-rise building structure at height $z\mathrm{m}$ is expressed by $\bar{D}(z)$, and the corresponding expected extreme value is expressed by $\hat{D}(z)$. The expected extreme value of structural displacement response is estimated by $\hat{D}(z)=\mu_{dis}+g\sigma_{dis}$, and the expected extreme value of structural acceleration response is estimated by $\hat{D}_{acc}(z)=g\sigma_{acc}$.

The reliability analysis theory of wind vibration response of super high-rise building under wind load is as follows: the wind direction frequency function $f(\theta)$ and the corresponding distribution function parameters are fitted by harmonic function, whose expression is:

$$f_o(\theta)=c^f+\sum_{m=1}^{n_t} d_m^f \cos\left(m\theta-e_m^f\right)$$

$$f_\theta(\theta)=c^f+\sum_{m=1}^{n_f} d_m^f \cos\left(m\theta-e_m^f\right) \tag{32}$$

$$a(\theta)=c^a+\sum_{m=1}^{n_a} d_m^a \cos\left(m\theta-e_m^a\right) \tag{33}$$

$$b(\theta)=c^b+\sum_{m=1}^{n_b} d_m^b \cos\left(m\theta-e_m^b\right) \tag{34}$$

In the above three equations, the frequency of any wind angle is expressed by $f_\theta(\theta)$; $a(\theta)$, $b(\theta)$ are the parameters in the distribution function; c, d_m, e_m are the parameters inside the harmonic function; n_f, n_a, n_b are the corresponding orders of the harmonic function.

The structural function function is constructed to carry out the reliability analysis of wind vibration response of super high-rise building structure:

$$Z_a=[a]-a_s \tag{35}$$

Among them, the acceleration limit value required by the specification is expressed in $[a]$. According to the specification ISO10137, when the structural self-oscillation frequency is 0.175Hz, the 50-year reproduction period for the top of the structure of the building acceleration response extreme value is not greater than $0.09m/s^2$, for the top of the structure of the office structure acceleration response extreme value is not greater than $0.13m/s^2$, and the top of the structure of the ultra-high-rise building peak acceleration is expressed in a_s.

It is assumed that the probability of exceeding the limit value under this wind angle at this time is equal to the probability of wind speed greater than the wind speed occurring under this wind angle in the joint distribution function of wind speed and wind direction for the corresponding reproduction period, that is:

$$P_{f_t}(f\mid\theta)=1-\exp\left[-\exp\left(-\frac{x-b(\theta)}{a(\theta)}\right)\right] \tag{36}$$

Then consider the total probability that the joint distribution of wind speed and direction exceeds the limit on a conditional probability basis P_f, which is expressed as:

$$P_f = \sum_{i=1}^{n} f(\theta) P_{f_i}(f \mid \theta) \tag{37}$$

The reliability of the super tall building structure under the 50-year return period considering the joint distribution of wind speed and direction is under the condition of meeting the comfort requirements:

$$Z_{a10} = \left[1 - P_f\right]^{10} \tag{38}$$

The extreme value of displacement response of the top floor of the super tall building structure at 50-year return period is obtained by calculation, which facilitates the construction of the structural function function to carry out the reliability analysis of the wind vibration response of the super tall building structure:

$$Z_d = [d] - d_s \tag{39}$$

Among them, the specification of the ultra-high-rise structure of the inter-story displacement angle limit value expressed in $[d]$, according to the current national standard high-rise building concrete structure technical regulations of the height of not less than 250m of high-rise building floor layer maximum displacement and the ratio of the height of the layer should not be greater than 1/500, d_s is the ultra-high-rise structure of the structure of the top layer of the maximum inter-story displacement and the ratio of the height of the layer.

If $Z_d > 0$, then judge that the wind angle under the wind response is reliable; if $Z_d < 0$, you can judge that the wind angle under the limit, assuming that the probability of exceeding the limit at this time:

$$P_f^d(f \mid \theta) = \left\{1 - \exp\left[-\exp\left(-\frac{x - b(\theta)}{a(\theta)}\right)\right]\right\} \frac{n}{69} \tag{40}$$

Where n is the number of floors where the inter-story displacement angle exceeds the limit at that wind angle. The total probability of exceeding the limit value calculated on the basis of conditional probability P_f i.e:

$$P_f^d = \sum_{i=1}^{n} f(\theta) P_{f_i}^d(f \mid \theta) \tag{41}$$

The reliability of the super high-rise building structure under a 50-year return period considering the joint distribution of wind speed and direction is:

$$Z_{d50} = \left[1 - P_f^d\right]^{50} \tag{42}$$

The reliability of the super high-rise building structure under 100-year return period considering the joint distribution of wind speed and direction is:

$$Z_{d100} = \left[1 - P_i^d\right]^{100} \tag{43}$$

3.3. Construction of Finite Element Model for Large-Span Steel Structures

3.3.1. Finite Element Modeling of Large-Span Steel Structures. This paper takes the trestle bridge as an example to improve the design

1) Engineering overview. This paper studies a five-span steel trestle bridge, with spans of 28m, 48.5m, 48.5m, 33.8m and 50m respectively, and hereafter narrated in this paper, all of which are expressed in terms of the first to the fifth spans to express their specific positions. The basic information of each span is shown in Table 1. According to the use of the central part of the trestle to set up a tape machine, and set up on both sides of the maintenance aisle, five spans of trestle width are 5.2 m. Steel structure trestle one end of the articulated support, one end of the sliding support.

Table 1. The basic information of each cross pier

Position	Span (m)	Star vector height (m)	Angle (°)	Height of climb (m)
First cross	28	4	13	5.85
Second cross	48.5	4	13	10.2
Third span	48.5	4	13	10.2
Fourth cross	33.8	4	13	6.55
Fifth cross	50	4	3	1.93

(1) Design parameters: the basic wind pressure of this project is $0.5kN/m^2$, and the roughness of the ground is B class;

(2) Design load: floor live load $3.5kN/m^2$, roof live load $0.5kN/m^2$;

(3) Structural material: steel truss, steel member, node plate are all made of Q235B steel. The principal relationship of Q235B steel adopts ideal linear elasticity model, which is isotropic material, i.e.: $EX = EY = EZ$.

The structural arrangement of the trestle is shown in Fig. 7.

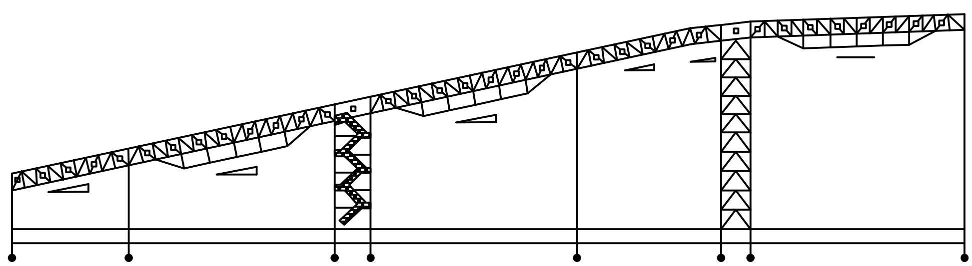

Fig. 7. Structure layout of the trestle

2) Model parameters. Unit cross-section type and parameters: the final detailed cross-section parameters of each major rod are shown in Table 2.

Table 2. Section characteristic

Model	Unit number	Unit type	A (mm2)	Ix (mm4)	Iy (mm4)
First cross Fourth cross	1	2L140x12	5410	1.02909E7	2.10824E7
	2	2L125x10	4810	7234997	1.4895E7
	3	2L110x10	4210	4854058	1.06632E7
	4	HW250x250x9x14	9228	1.08E8	3.65E7
	5	L100x8	1573.8	1482410	1482410
	6	Work 16	2623.1	1.13E7	931010
	7	2L125x8	3882	5923278	1.18783E7
	8	HM300x200x8x12	7313	1.14E8	1.6E7
Second cross Third span Fifth cross	9	2L180x16	11018	3.41284E7	7.10406E7
	10	2L110x10	4210	4854058	1.06632E7
	11	2L125x10	4810	7234997	1.4895E7
	12	2L160x14	8578	2.10149E7	4.43345E7
	13	2L180x16	11018	3.41284E7	7.10406E7
	14	HW300x300x10x15	12050	2.05E8	6.76E7
	15	L100x10	1936.1	1795110	1795110
	16	Work 16	2623.1	1.13E7	931010
	17	L100x8	1573.8	1482410	1482410
	18	L125x12	2901.2	4231610	4231610
	19	HM300x200x8x12	7313	1.14E8	1.6E7
	20	HW150x150x7x10	3975	1.62E7	5630010

3) Modeling. There are frame unit, shell unit, connection unit and solid unit in the finite element analysis software Sap2000, which are combined together and after a series of assumptions, can simulate the force of the complex real structure. The trestle structure mainly uses frame units, which are used to simulate beams, column supports and trusses in the structure. The frame unit uses the classical 3D beam-column formulation, and Sap2000 can simulate a variety of mechanical forms, including the effects of axial edge, torsion, biaxial bending and biaxial shear deformation. In order to try to ensure that the model fits the actual structure, according to the structural characteristics of the trestle bridge, with reference to the actual construction drawings and combined with the relevant specifications and design manuals, the following linking methods are used for each component in the model building process:

(1) End portal frame column foot node degrees of freedom are released in accordance with the structural design, the articulated end releases the moment degrees of freedom in three directions, and the sliding end releases the X-direction shear force without taking into account the friction force of the sliding support in this paper.

(2) The steel structure tower is completely rigidly connected with the foundation.

(3) The truss bridge body part, web rods, upper and lower horizontal supports are articulated according to the design.

3.3.2. Determination of the damping term. The research model in this paper uses the Rayleigh damping model [24] for the damping setting. The Rayleigh damping model, also known as proportional damping, is a simpler form of modeling commonly used today, and its accuracy is sufficient for practical engineering, with the mathematical expression shown below:

$$[C]=\alpha[M]+\beta[K] \tag{44}$$

$$\begin{bmatrix} \xi_i \\ \xi_j \end{bmatrix} = \frac{1}{2} \begin{bmatrix} \frac{1}{\omega_i} & \omega_i \\ \frac{1}{\omega_j} & \omega_j \end{bmatrix} \begin{bmatrix} \alpha \\ \beta \end{bmatrix} 0 \tag{45}$$

Where: $[M]$ is the mass matrix;
$[K]$ is the stiffness matrix;
$[C]$ is the structural damping matrix;
ξ_i, ξ_j, is the damping ratio;
ω_i, ω_j are the angular frequencies;
α, β are the mass matrix coefficients and stiffness matrix coefficients.

According to the determination of Rayleigh damping coefficient there are four methods of determining, and through simulation and comparison, the calculation results of Rayleigh damping coefficient of the four methods are similar, the structural response does not appear oscillation phenomenon, the fitting effect is better.

It is assumed that: the contribution of mass matrix and stiffness matrix to the Rayleigh damping is equal. Then there are:

$$\alpha = \xi\omega_1, \beta = \xi / \omega_1 \tag{46}$$

From the modal analysis to find the first formation cycle is $T_1 = 2.079$, so the circular frequency $\omega_1 = 2\pi / T_1 = 3.021$, and the structure of the damping ratio of $\xi = 0.04$, substituting into the above equation, get:

$$\alpha = 0.121, \beta = 0.0132 \tag{47}$$

4. Analysis of the results of the dynamic characterization of the wind resistance of the improved long-span steel structure

4.1. Finite Element Analysis of Wind Vibration for Example of High-Rise Assembled Structure Project

4.1.1. Structural modal analysis. Structural practical engineering, the structure was modeled and the first 10 orders of vibration modes of the structure were calculated using ETABS.

1) Self-oscillation period and frequency analysis of the structure. This paper mainly extracts the first 10 orders of self-oscillation period and frequency of ETABS model. The first 10 orders of self-oscillation frequency and period of the assembled structure are shown in Fig. 8. It can be found that with the increase of the number of layers, each cycle gradually increases, but there is a tendency to decrease at T1p/T1c. For the convenience of practical engineering design, the average value of the three is taken, i.e., the cycle enhancement coefficient of the assembled structure compared with the cast-in-place structure is 1.182.

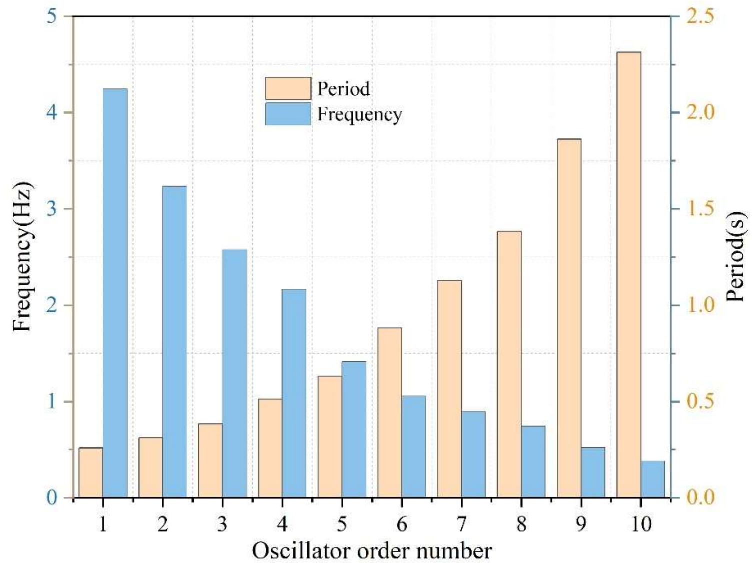

Fig. 8. The first 10 order vibration frequency and period of the assembly structure

The design results structural period with ETABS calculation are shown in Fig. 9. The first three orders of the period of the assembled structure are T1=2.1017s, T2=1.6255, and T3=1.2726.From the figure, it can be found that the design results obtained the self-oscillating period which is smaller than that calculated by ETABS.

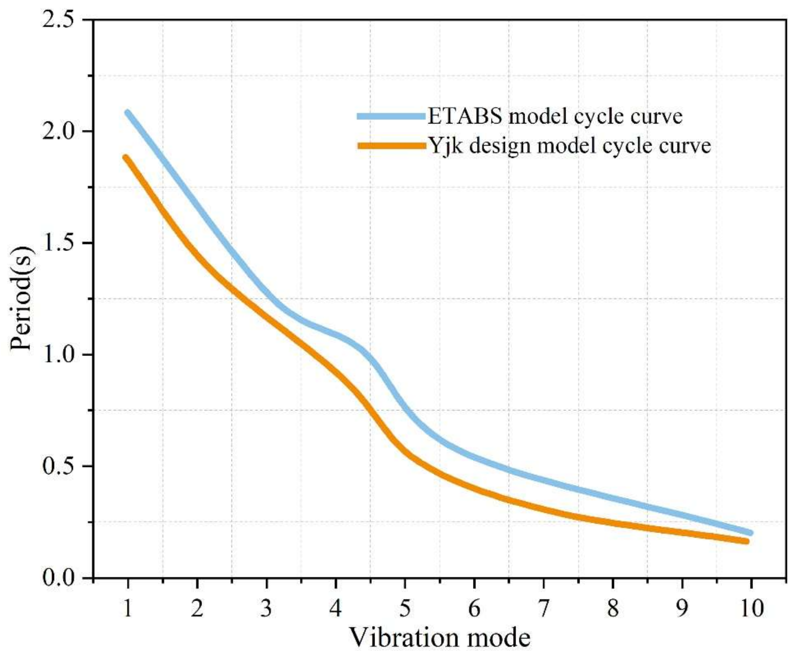

Fig. 9. Design results structure cycle and ETABS calculation results

2) Comparison of cycles of cast-in-place and assembled structures. 10-span and 22-span cast-in-place and assembled self-oscillation cycle shown in Table 3, the comparison of cast-in-place structure and assembled structure can be found: their vibration pattern is dominated by the first vibration type of advection, but there are some differences between the two T1, T2 and Tt, and the cycle of assembled structure is slightly larger.

Table 3. 10 span and 22 span current and assembly type self-oscillation cycle

Structural type	T1	Tt	T2	Tt/T1
10 span	0.5573	0.4345	0.4458	1.0201
22 span	0.6486	0.4924	0.5181	0.9658
10 span	1.9609	1.2371	1.447	0.6992
22 span	2.1687	1.3416	1.6965	0.6804

The period of 5-span, 10-span and 21-span structures are shown in Table 4. From the table, it can be seen that the first vibration pattern of the assembled structure belongs to the advection along the y-direction, and the period is obviously larger than that along the x-direction in the second vibration pattern, and it is learned that there are certain differences in the stiffness of the structure in the x- and y-directions, and the x-direction is obviously larger than that in the y-direction. The second vibration pattern belongs to the x-direction slightly torsion of the advection, the third vibration pattern belongs to the torsion vibration, the fourth vibration pattern belongs to the bending vibration, from the fourth vibration pattern onwards are flat and torsion coupling vibration.

Table 4. The cycle ratio of the 5&10&21 layer structure

Layer number	T1p	T1c	T1p/T1c
5	0.3319	0.3621	1.0910
10	0.7026	0.6783	0.9654
21	2.2227	2.0819	0.9367

4.1.2. Calculation of wind vibration response:

1) Comparison of simulation results and design results. Comparison of design results and ETABS structural displacements under wind load is shown in Fig. 10, with (a) and (b) showing the displacements in x-direction and y-direction, respectively. From the figure, it can be seen that the maximum displacement of the ETABS model in the y-direction under a 50-year wind load is 18.72 mm, and the maximum displacement in the x-direction is 11.65 mm. The displacement curves in the x- and y-directions in the deformation and displacement diagrams show that the deformation of the structure in the y-direction under the wind load is larger than that in the x-direction.

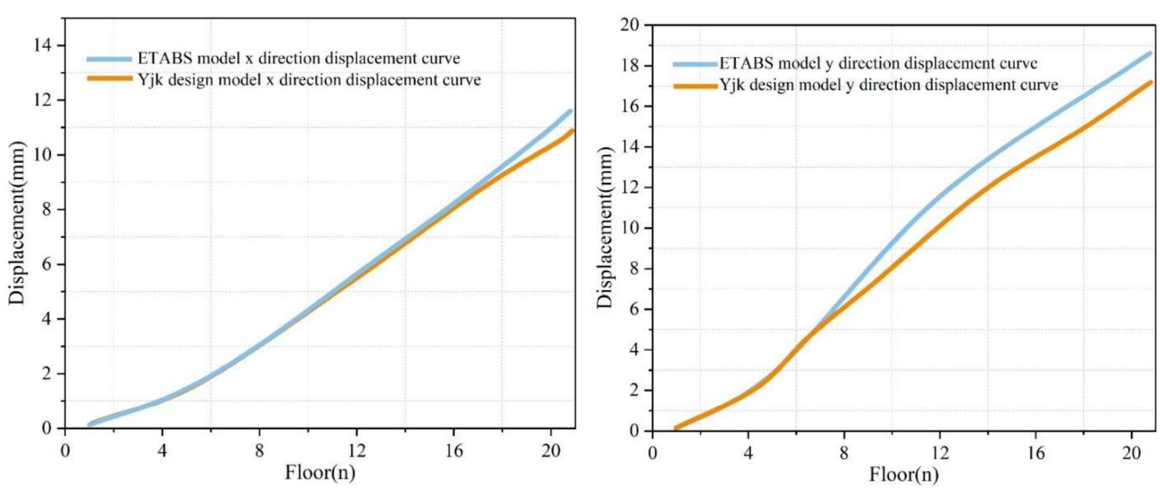

(a)x direction (b) y direction

Fig. 10. Design results and ETABS structure displacement contrast

The design results and ETABS inter-span displacement angles under wind load are shown in Fig. 11, with (a) and (b) referring to the y-direction and x-direction, respectively. From the figure, it can be seen that the inter-span displacement angle in the y-direction is 2.65 × 10-4, which satisfies the 1 × 10-4 limit required by the code.

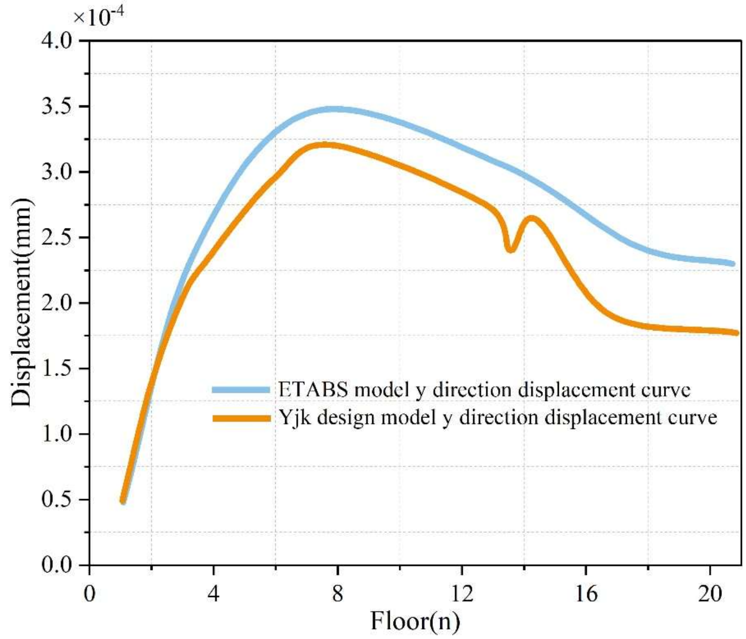

(a)y direction

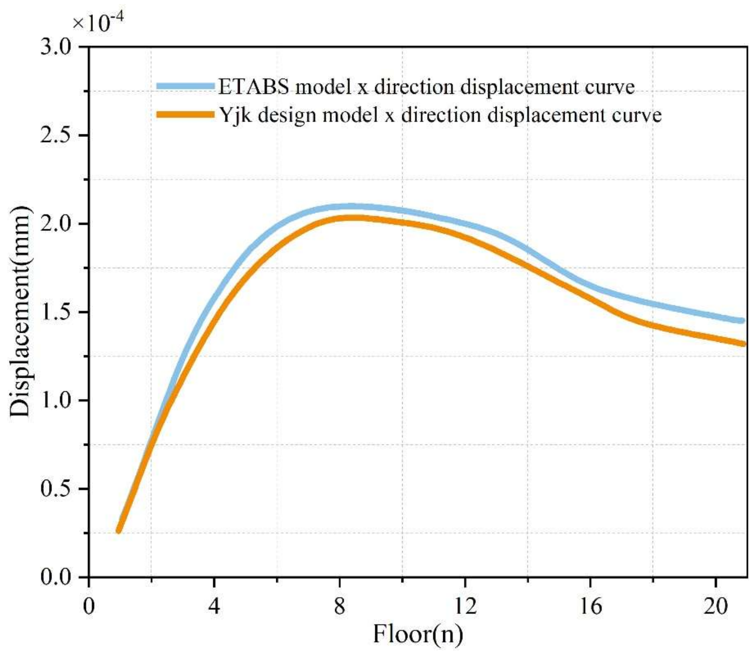

(b)x direction

Fig. 11. The displacement Angle between the wind load action and the ETABS layer

The results of the comparison between the design results under wind load and the acceleration of the ETABS structure are shown in Table 5. Comparison of design results under wind load and ETABS structural x and y acceleration found that the x-direction acceleration is smaller than the y-direction, and the x- and y-direction accelerations in the ETABS calculation results meet the comfort requirements. Comparison between the two found that the ratio of ETABS calculated wind vibration response to the design results is 1.182, so in the wind design, it is recommended that the structural wind vibration calculation should be multiplied by an increase factor of 1.182.

Table 5. The design results were compared with the ETABS structure acceleration

Calculation method		Yjk design results	ETABS calculation results
Downwind	X direction	0.200	0.038
Acceleration m/s^2	Y direction	0.261	0.109

2) Wind vibration parameter analysis. The wind vibration response was analyzed above for the selected engineering examples and cast-in-place structures respectively, and the applied loads were pulsating wind loads in the case of one in 50 years. In order to further investigate the wind vibration response of high span assembled structures, the wind vibration response of assembled structures is investigated by varying the change in wind speed to which the structure is subjected. The basic wind pressure w0=0.5kN/m2 and the corresponding basic wind speed v=27.5m/s for the one-in-50-year wind speed are shown in Fig.12. (a) is the acceleration at the top of the structure for the one-in-50-year wind speed, and (b) is the peak displacement at the top of the structure for the one-in-50-year wind speed. When subjected to a wind speed of one in 50 years, the amplitude of the acceleration time curve of the top structure is between ±0.08, which meets the comfort requirements of the high code. If the top floor meets the requirements, the overall comfort level also meets the requirements. Generally within the gradient wind height, the wind vibration response of the bridge increases with height, mainly because the higher the height the higher the wind speed. However, in the case of high spans, if the top span structure meets the specification requirements, the overall comfort level meets the requirements. Moreover, as the wind speed parameter changes, the acceleration response at the top of the structure increases with the wind speed.

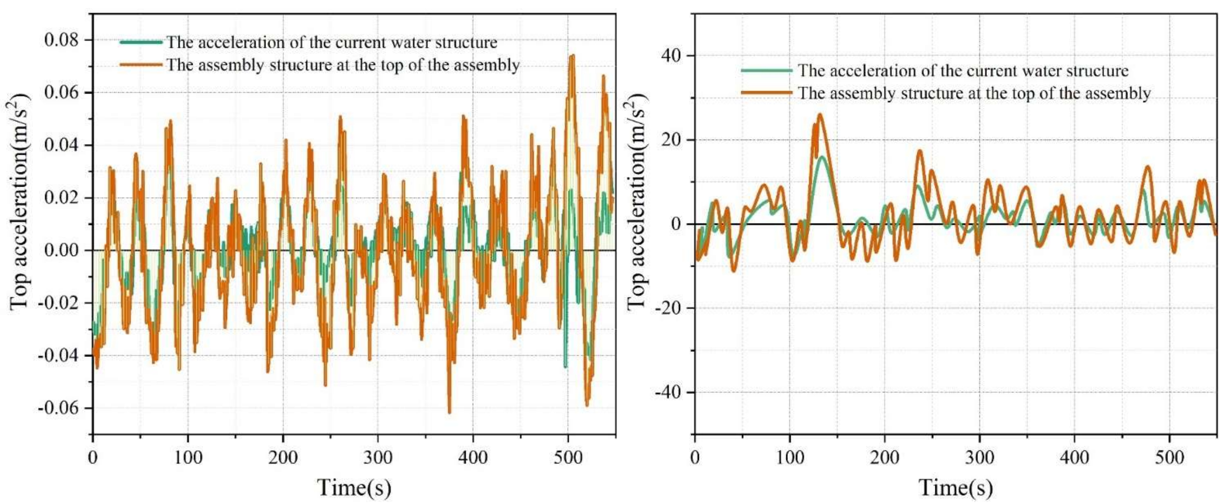

(a)Top acceleration of wind speed structure (b)Peak displacement of wind speed structure

Fig. 12. The results of the wind wind structure at the top of 50 years

4.2. Dynamic characterization of wind performance of long-span steel structures

The results of the comparison of the displacements of each layer under mean wind action after optimization of the reinforcement layer are shown in Fig. 13. It shows the comparison of the displacements of each layer under the average wind action after optimizing the reinforcement layer according to Method I (stepwise approximation method) and Method II (continuum topology optimization). From the figure, it can be seen that the displacements of each layer of the structure under average wind action after arranging the reinforcement layer according to Method 2 are not much different from those of Method 1, and the corresponding displacements of the top layer of Methods 1 and 2 are 0.1685 m and 0.1749 m, respectively, which are less than 0.2 m and satisfy the minimum stiffness requirement of the structure. This indicates that both methods have achieved the expected effect of increasing the overall stiffness of the structure.

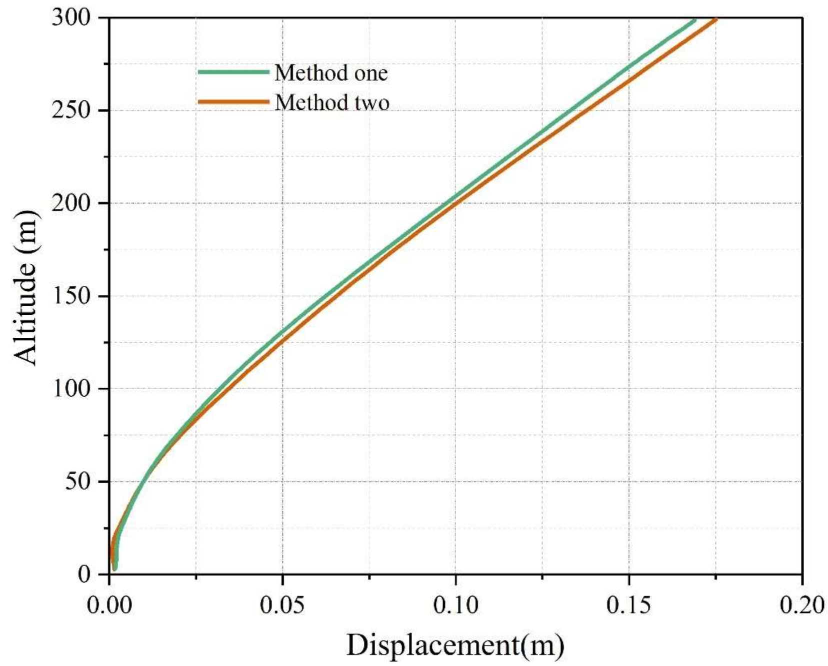

Fig. 13. The contrast results of the average wind effect of the layer are optimized

The displacement of each layer of downwind action after optimization of the reinforced layer is shown in Fig. 14. The acceleration of each layer under downwind action after optimization of reinforced layer is shown in Fig. 15. The peak displacements and accelerations of each layer are compared with the peak values of each layer under the downwind action after the optimization of the reinforced layer. As can be seen from the figure, after arranging the reinforcement layer according to the two methods, the peak values of displacement and acceleration of each layer of the structure arranged according to method 1 are slightly smaller than those arranged according to method 2 under downwind action. This indicates that the contribution of the reinforcing layers to the overall stiffness of the structure arranged by Method 1 is better than that of Method 2. The peak displacements of the top storey under downwind action corresponding to Methods I and II are 0.5005m and 0.5245m, respectively, which are both larger than 0.4m, and do not meet the structural design stiffness requirements. The peak acceleration of the top layer corresponding to the downwind action of Method I and Method II are 0.2286m/s^2 and 0.2386m/s^2, respectively, which are both greater than 0.15m/s^2, and do not satisfy the requirement of structural design comfort.

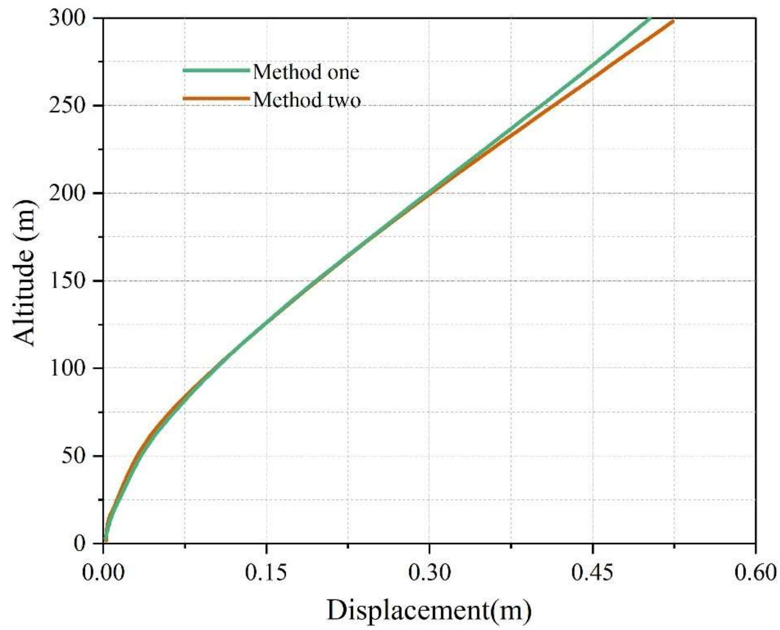

Fig. 14. The strengthening layer is optimized and the wind is displaced by the wind

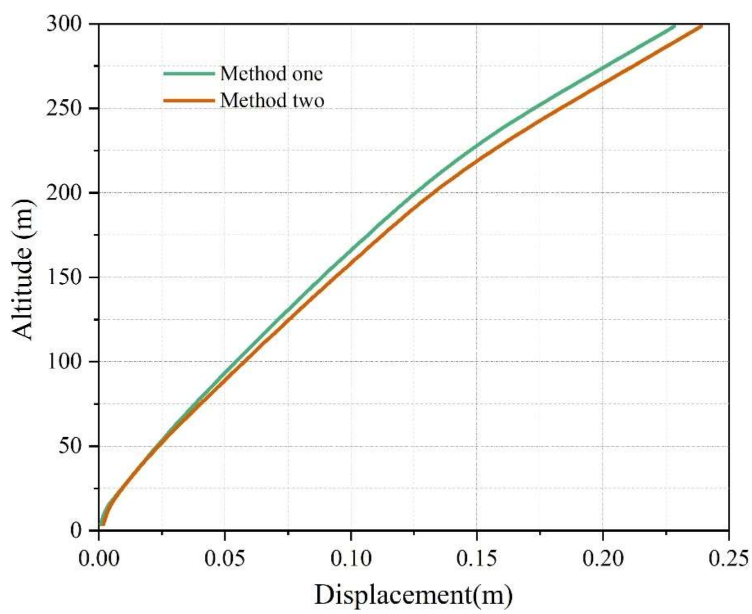

Fig. 15. Optimization of the various layer acceleration after the wind

The comparison of the displacement of the top layer of the structure under downwind is shown in Fig. 16; the comparison of the acceleration of the top layer of the structure under downwind is shown in Fig. 17. As can be seen from the figure, after continuing to arrange the reinforcement layer damping system in the optimal position according to Methods 1 and 2, the peak values of the displacement and acceleration of each layer of the structure under the action of downwind are still not much different, which indicates that the optimized arrangement of the reinforcement layer damping system with the corner amplitude of each layer of the core cylinder as the objective function can achieve the same good effect as the optimization of the continuum topology. There are two main reasons: Method 1 has a better effect on the overall stiffness of the structure than Method 2, and the overall stiffness of the structure leads to a reduction of deformation, which affects the control effect of the damper on the wind vibration; Method 2 takes the corner amplitude of each layer of the structural core as the objective function, while Method 1 takes the peak displacement and acceleration of the top layer of the structure and the weight of the peak value of the acceleration as the objective function, which makes the optimized result of Method 2 better than Method 1 in terms of the reduction of acceleration. This also makes the optimization result of method II better than method I in terms of acceleration reduction.

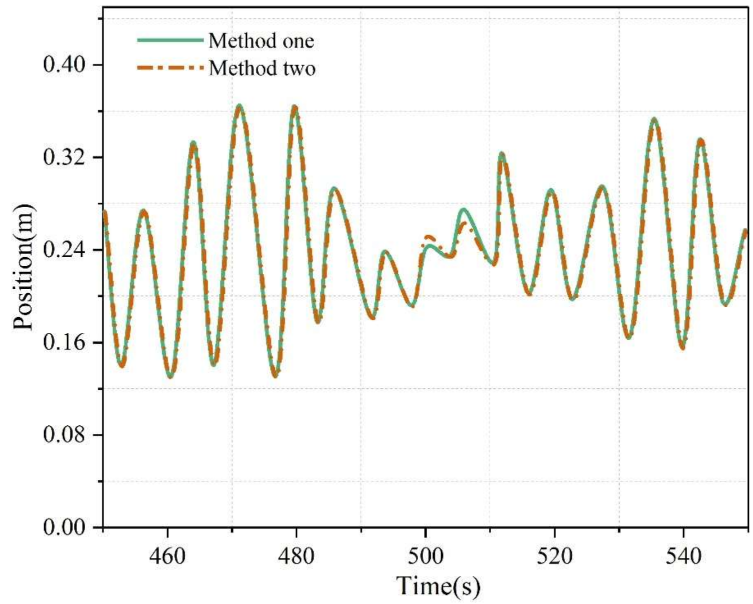

Fig. 16. Contrast of the displacement interval of the low-wind structure

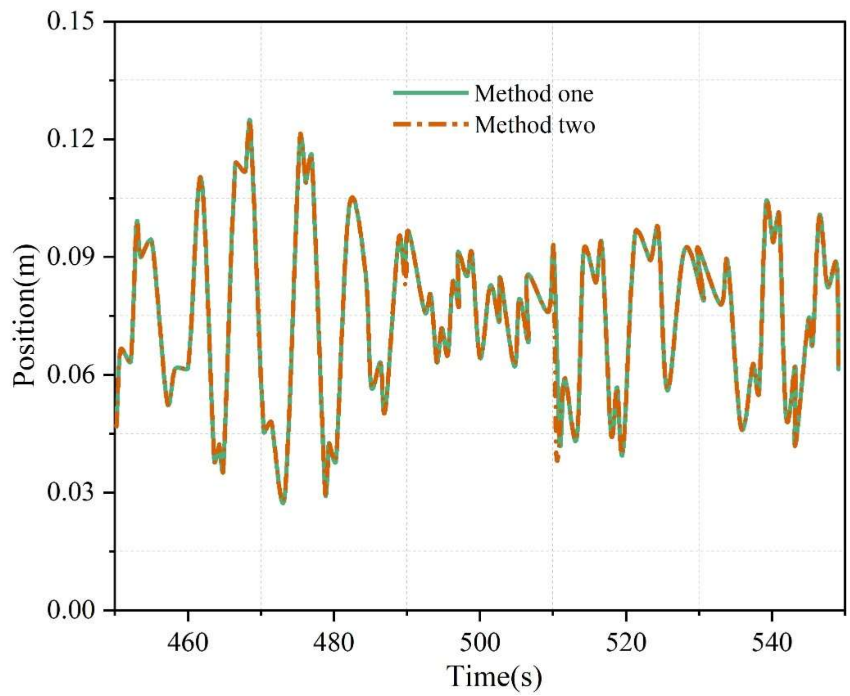

Fig. 17. Contrast of the high level acceleration of the lower wind structure

Fig. 18 shows the comparison results of the total input energy of wind vibration; Fig. 19 shows the comparison results of the total absorbed energy of the main structure; and Fig. 20 shows the comparison results of the additional damping dissipation energy. As can be seen from the figures, the total input energy of wind vibration of the structure after the optimised arrangement of the two methods is almost equal, the total absorbed energy of the main structure after the optimised arrangement of Method 2 is slightly lower than that of Method 1, and the additional damping dissipation energy of Method 2 is slightly higher than that of Method 1. This indicates that the optimised arrangement according to Method 2 can make the dampers give fuller play to the energy dissipation and vibration reduction. From the energy point of view, the optimised arrangement of Method 2 is better than that of Method 1.

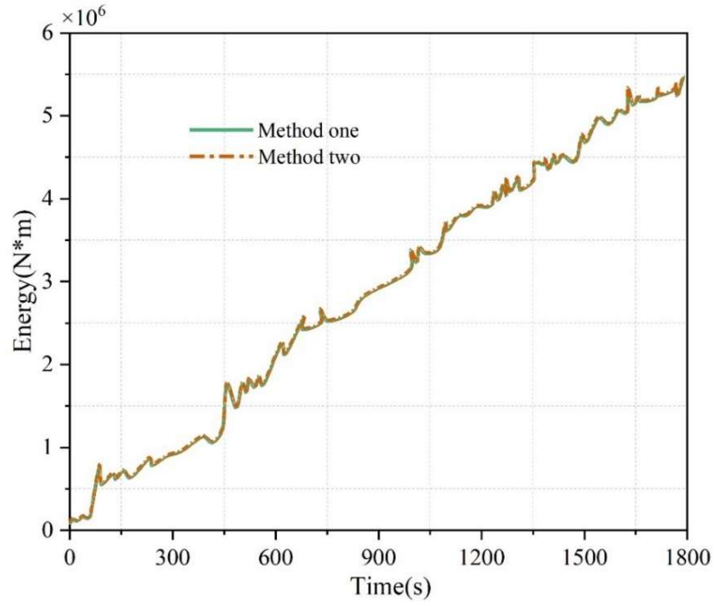

Fig. 18. The results of the total input can be compared

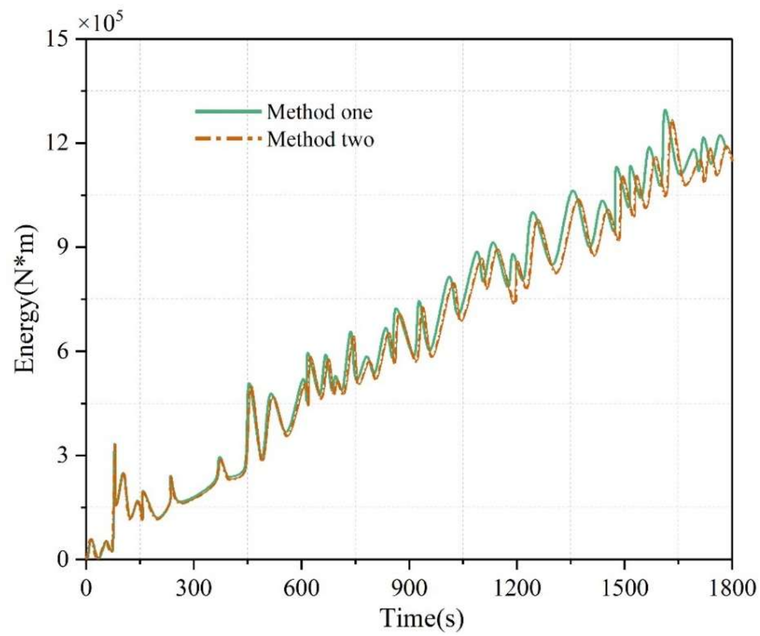

Fig. 19. The total absorption of the main structure is compared to the result

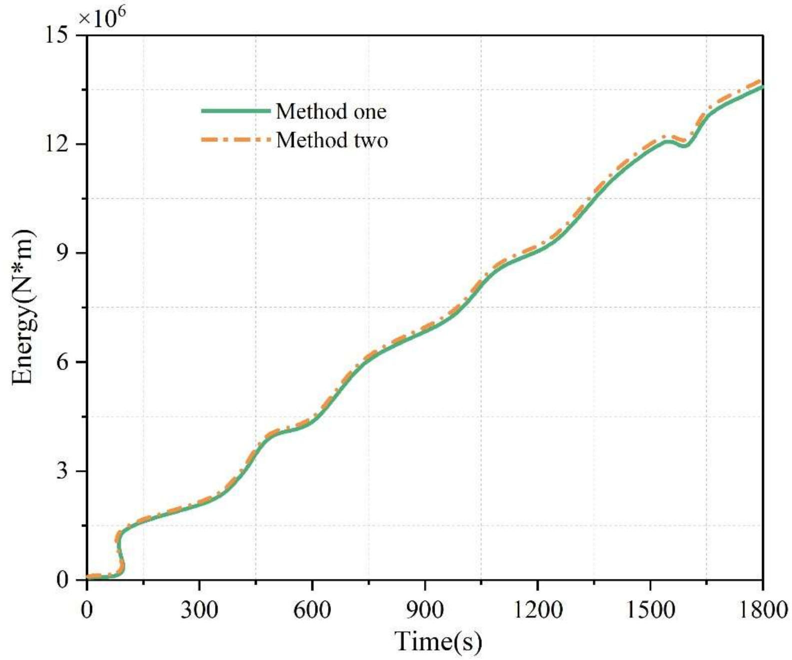

Fig. 20. The additional damping dissipated time range comparison results

4.3. Modification of the optimised structural model and checking analysis

4.3.1. Self-weight load analysis and modal calculation. In this paper, based on the principle of symmetrical distribution of diagonal braces as much as possible, the optimized structural model is modified, i.e., the placement of diagonal braces is fine-tuned to redistribute them. A small amount of diagonal strut members are added to obtain the modified structure (hereinafter referred to as "modified structure"). Modal analysis is performed to obtain the first six orders of the modified structure model, and the first six orders of the modified structure model are shown in Table 6. It can be seen that the fixed frequencies of each order of the modified structure are higher than the fixed frequencies of each order of the extended-arm damping and lower than the fixed frequencies of each order of the extended-arm truss structure.

Table 6. Correct the first six order of the structure model

Frequency	Numerical value
First-order frequency	0.6854
Second-order frequency	0.7023
Tristage frequency	0.9941
Quaternary frequency	1.5847
Pentapoquinary frequency	21362
Hexadinian frequency	2.7497

4.3.2. Structural response under wind loading. Through the calculation and analysis, the node displacements of each floor of the modified structure model are extracted, and the node displacements of each floor of the modified structure model are shown in Fig. 21, with (a) and (b) being the X-direction and Y-direction, respectively. It can be seen that the node displacement of the top floor is 0.0098m after the wind load in X direction is applied to the model, and 0.0165m after the wind load in Y direction is applied to the model, which are much smaller than the requirement of 1/500 of the limit value of horizontal displacement of the top floor of the frame structure.

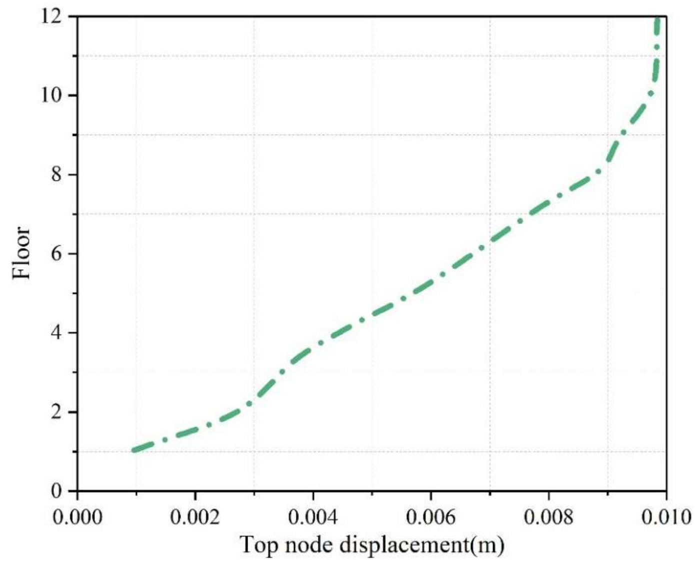

(a) X direction

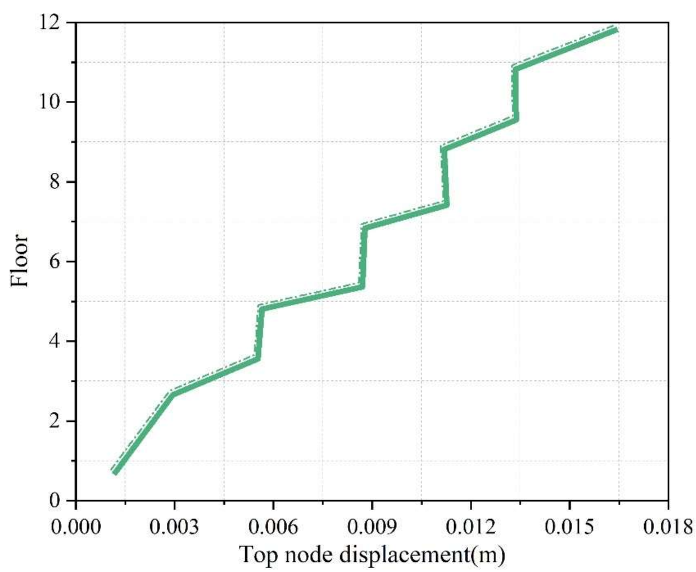

(b) Y direction

Fig. 21. Modify the displacement of each floor of the structural model

After analyzing and calculating, the inter-story displacement angle of the modified structural model is obtained as shown in Fig. 22, (a) and (b) are the X direction and Y direction respectively. It can be seen that the maximum inter-story displacement angle in the X direction occurs in the 1st floor, and the maximum inter-story displacement angle in the Y direction occurs in the 5th floor, with the values of 0.00042 and 0.00097 respectively, which satisfy the requirement of less than the limit value of the inter-story displacement angle of frame structure of 1/420. And the calculation results are close to those of full diagonal bracing, which proves that the design of the modified structural mode is reasonable and effective.

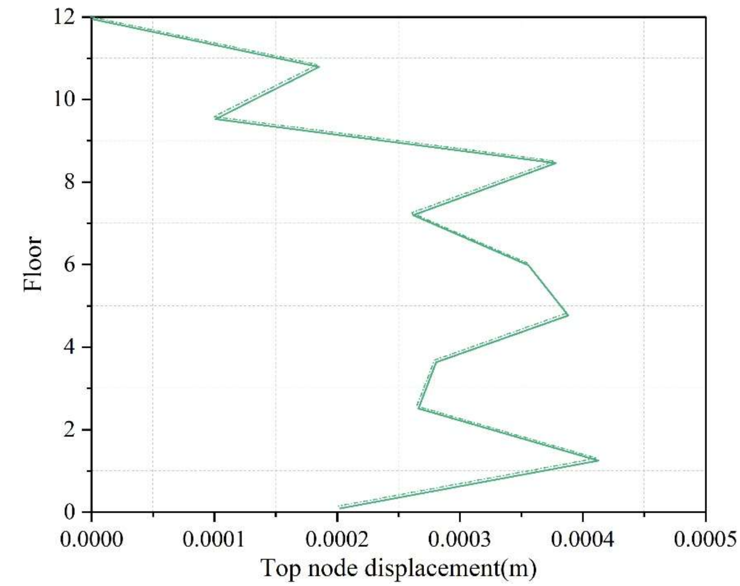

(a) X direction

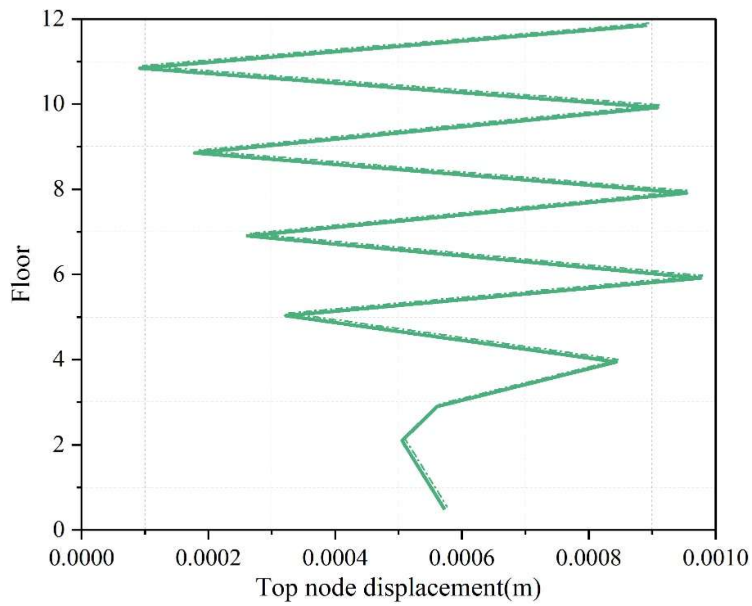

(b) Y direction

Fig. 22. Modified structural model of interlayer displacement Angle

5. Conclusion

Based on the topology optimization theory and combined with the wind vibration control principle, this paper carries out an in-depth research on the design theory for improving the dynamic characteristics of wind-resistant performance of large-span steel structures. The research results provide theoretical support and reference design for the wind-resistant design of large-span steel structures.

1) In this paper, a reasonable ETABS finite element model is established to simulate the high-rise assembled structure in combination with the actual project, and the wind load simulation results are applied to the model and modal analysis and wind vibration response analysis are carried out, and compared with the design results, and the cast-in-place structure and the assembled structure are

compared by changing the wind speed parameter, so as to verify the rationality of the assembled structure.
2) According to the wind vibration response of the structure, the effect of using continuum topology optimization to optimize the reinforcement layer is better than the effect of optimizing the optimal position arrangement according to finite element software. It is feasible and effective to optimize the damping system of the reinforcement layer with the corner value of each layer of the core as the objective function. The reinforcement layer arrangement only needs to meet the minimum stiffness of the structure to give full play to the wind vibration damping effect of the reinforcement layer damping system. The continuum topology optimization can be combined with the value of the objective function to fully consider the functional requirements of the building, so that engineers and technicians can get a more reasonable layout in the preliminary design stage.
3) The displacement and interstory displacement angles of each layer of the structure under wind load are calculated, and after finding that the interstory displacement angle does not meet the design requirements of less than 1/420, the optimization model is modified, and the displacement and interstory displacement angles of each layer node under the wind load of the modified structural model are checked, and the results meet the top displacement limit and the interstory displacement angle limit, and the performance is similar to that of the outrigger truss structure model.

Funding

This work was supported by Projects of Industry-Education Collaborative Education of the Ministry of Education (220604276301812).

References

[1] Li, L. (2022). Long-span Steel Structure System and Application Case Summary. Highlights in Science, Engineering and Technology, 18, 155-161.

[2] Han, T., Liang, S., Zhu, X., Wang, W., & Yang, J. (2023). An investigation of the flexural behaviour of large-span prestressed and steel-reinforced concrete slabs. Scientific Reports, 13(1), 10710.

[3] LEI, S. S., LIU, Y. F., DUAN, X. J., GUO, X. H., LI, X. F., LI, J. H., ... & NIE, X. (2018). Study of comprehensive monitoring technology of the construction process of complex large-span spatial steel structures. Engineering Mechanics, 35(12), 203-211.

[4] Fairclough, H. E., & Gilbert, M. (2022). Layout optimization of long-span structures subject to self-weight and multiple load-cases. Structural and Multidisciplinary Optimization, 65(7), 197.

[5] Dong, S., Zhao, Y., & Xing, D. (2012). Application and development of modern long-span space structures in China. Frontiers of Structural and Civil Engineering, 6, 224-239.

[6] Krishna, P. (2021). A review of developments in steel: Implications for long-span structures. Transactions of the Indian Institute of Metals, 74(5), 1055-1064.

[7] Pan, W., Turrin, M., Louter, C., Sariyildiz, S., & Sun, Y. (2019). Integrating multi-functional space and long-span structure in the early design stage of indoor sports arenas by using parametric modelling and multi-objective optimization. Journal of Building Engineering, 22, 464-485.

[8] Yao, G., Li, R., Yang, Y., Cai, X., Zhou, Y., Zhou, C., & Lei, T. (2024). Analysis of Mechanical Properties during Construction Stages Reflecting the Construction Sequence for Long-Span Spatial Steel Structures. Buildings, 14(8), 2389.

[9] Luzenina, I., & Sosnovskikh, L. (2022, October). Steel space frame structures of long-span buildings. In AIP Conference Proceedings (Vol. 2657, No. 1). AIP Publishing.

[10] Hui, C., Jiao, Y., Liu, M., & Hai, R. (2023). Investigation and analysis of stress and deformation monitoring of long-span steel roof trusses. Buildings, 13(2), 398.

[11] Olga, P., Pavel, C., Alexey, L., & Chafic-Touma, S. (2022). Stability and reliability of long-span bridge structures. Architecture and Engineering, 7(3), 65-75.

[12] Simiu, E., & Yeo, D. (2019). Wind effects on structures: Modern structural design for wind. John Wiley & Sons.

[13] Zhou, Y., & Sun, L. (2018). Effects of high winds on a long-span sea-crossing bridge based on structural health monitoring. Journal of Wind Engineering and Industrial Aerodynamics, 174, 260-268.

[14] Zhao, Z., Liu, H., & Chen, Z. (2017). Field monitoring and numerical analysis of thermal behavior of large span steel structures under solar radiation. Advanced Steel Construction, 13(3), 190-205.

[15] Lu, C., Yang, Z., Zheng, L., & Liu, Z. (2023). Smart Reliability Analysis of Wind Resistance of Lightweight Steel Structures in Super Tall Buildings in a Smart City. Journal of Testing and Evaluation, 51(3), 1793-1803.

[16] Han, Y., Li, K., Cai, C. S., Wang, L., & Xu, G. (2020). Fatigue reliability assessment of long-span steel-truss suspension bridges under the combined action of random traffic and wind loads. Journal of Bridge Engineering, 25(3), 04020003.

[17] Li, S., Laima, S., & Li, H. (2017). Cluster analysis of winds and wind-induced vibrations on a long-span bridge based on long-term field monitoring data. Engineering Structures, 138, 245-259.

[18] Fang, G., Pang, W., Zhao, L., Xu, K., Cao, S., & Ge, Y. (2022). Tropical-cyclone-wind-induced flutter failure analysis of long-span bridges. Engineering Failure Analysis, 132, 105933.

[19] Fenerci, A., & Øiseth, O. (2017). Measured buffeting response of a long-span suspension bridge compared with numerical predictions based on design wind spectra. Journal of Structural Engineering, 143(9), 04017131.

[20] Liang Yujia,Zhang Yuxin,Wen Zhe,Du Yalong & Chen Shujin. (2021). Wind Load Electrically Controlled Automatic Assembly through Computer BIM Model. Journal of Physics: Conference Series(1),

[21] Jia Ruofan,Ji Xiaodong,Cheng Yuhao & Ikago Kohju. (2023). Seismic response control of core wall structures using tuned viscous mass damper (TVMD) outriggers. Engineering Structures

[22] Zhen Liu & Liang Xia. (2025). Feature-driven topology optimization of continuum structures with tailored octree meshing. Finite Elements in Analysis & Design104308-104308.

[23] Guixing Li & Yuan Chen. (2025). Highly efficient and extensible parallel topology optimization for continuous fiber reinforced composites. Computer Methods in Applied Mechanics and Engineering117713-117713.

[24] FaridGhahari,KhachikSargsyan & ErtugrulTaciroglu. (2024). Quantification of modeling uncertainty in the Rayleigh damping model. Earthquake Engineering & Structural Dynamics(9),2950-2956.